Chapter 12
Excited States Processes in Protonated Molecules Studied by Frequency-Domain Spectroscopy

Jennifer Noble, Claude Dedonder-Lardeux and Christophe Jouvet

In Protonated phenylalanine or tyrosine
Optical excitation leads to electron transfer from the aromatic ring to the NH_3^+ or to the carbonyl
which triggers
* H loss
* H transfer to CO then $CO+H_2O$ loss
* H transfer to the ring then C_α-C_β bond breaking

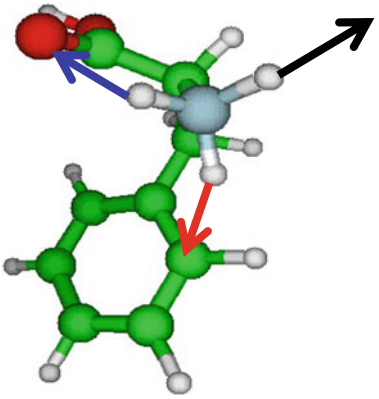

T. Ebata and M. Fujii (eds.), *Physical Chemistry of Cold Gas-Phase Functional Molecules and Clusters*,
https://doi.org/10.1007/978-981-13-9371-6_12

Abstract In this chapter we will review the processes at play in the excited states of protonated molecules. More specifically, the discussion will be restricted to aromatic molecules, on which the majority of studies have been focused. Rather than going into details of each system, we will highlight the trends and general mechanisms that are involved in the excited state energy and dynamics. The interested reader can find detailed descriptions of each molecule in the individual publications. It appears that the excited state dynamics of many aromatic ions can be understood upon the application of rather elementary and universal concepts, the simplest of which being that the excited electron is attracted to the proton, triggering a large part of the excited state dynamics.

Keywords Protonated molecules · Excited states dynamics · Ions trap · Fragmentation

12.1 Overview

The field covered in this chapter is the excited state properties of protonated aromatic molecules and simple systems, with the larger ones like peptides tackled in other chapters of this book. Here, we review studies performed over the last 10 years by various research groups around the world. It is interesting to begin by noting that this field has really exploded during that period; only two papers had been published prior to the year 2000 [1, 2]. The ground state structure of these ions has, on the contrary, been relatively well studied by infrared spectroscopy and vibrational analysis, and the reader can find out more by consulting recent reviews [3–5].

Let's start by stating some very simple concepts concerning the basic properties of protonated molecules: they are positively charged closed-shell molecules, with the same number of electrons as their neutral homologues. As such, when the proton is located on a substituent, one would not expect significant changes to the electronic states as compared to the neutral molecule. Since they are closed-shell molecules, ab initio calculations are quite reliable, and methods such as Couple Cluster (CC2) or time-dependent DFT give results that compare well with the experiments. Calculations are very precious in rationalizing the non-radiative processes induced during experimentation. We will describe below how, upon excitation, the excited electron tends to move to the positive charge, creating a locally hypervalent structure. If the proton is on a substituent (in this example, C–NH_3^+), then addition of an electron leads to the formation of a hypervalent C–NH_3 group which is highly unstable (as is NH_4) [6] and leads to the loss of an H atom. In large polyatomic molecules, charge transfer (CT) states can become the lowest excited state, which results in a strongly red-shifted electronic absorption.

J. Noble · C. Dedonder-Lardeux · C. Jouvet (✉)
PIIM, UMR-CNRS 7345, Aix-Marseille University Marseille, Marseille, France
e-mail: christophe.jouvet@univ-amu.fr

12.2 Experimental Methods

12.2.1 Ion Trap

Methods involving ion traps have been thoroughly discussed in the previous chapter, and in particular cold ion traps, which represent a kind of universal tool. Let us reiterate a few advantages of studying ions compared to neutral molecules. The first one is that ions can be kept for a very long time. Thus, the study of their dynamics is not limited in time, and systems can be followed from the femtosecond time scale, for the excited state dynamics, up to seconds, which often corresponds to the fragmentation of the ion or to secondary fragmentation. Since the ions are cold, electronic and/or IR spectroscopy allows the selection of isomers, tautomers, or conformers from well-resolved vibrational/electronic transitions.

Detection is achieved via fragmentation of the parent ion, measuring either the parent ion depletion or the fragment ion appearance. This means that the parent ions which have a fluorescence quantum yield of 100% will not be detected (but luckily this is never the case for large molecules) and that low-lying excited states (i.e. below the dissociation limit) cannot be detected via a one-photon process. On the contrary, systems which undergo very fast, non-radiative processes that are difficult to observe in case of neutral molecules (by fluorescence or multiphoton ionization) are easily detected in the case of ions. The fact that one vibronic level can be selectively excited in a well-defined system allows the use of the measurement of lifetime broadening as a tool to measure very fast (fs) processes even without femtosecond lasers.

12.2.2 Time-Resolved Experiments [7–9]

Pump/probe femtosecond (fs) experiments for neutral molecules rely on the ionization process detecting the ion or/and the electron. Protonated ions are already singly charged and are generally not ionized further due to their very high IP; instead they mostly undergo fragmentation. Detection then relies on the change of the fragmentation pattern upon the opening of new fragmentation channels or the modification of their relative branching ratio upon absorption of the probe laser. It should be noted that, for a system which has only one fragment, the absorption of the probe photon changes the fragmentation rate but not necessarily its efficiency and thus no dynamics can be observed. In the example given below (Fig. 12.1) for protonated tryptophan, one can see that the observed time evolution is different for each fragmentation channel. These data are very rich in information but quite tricky to understand and require more clues, such as fragmentation dynamics and ab initio calculations (vide infra) [10].

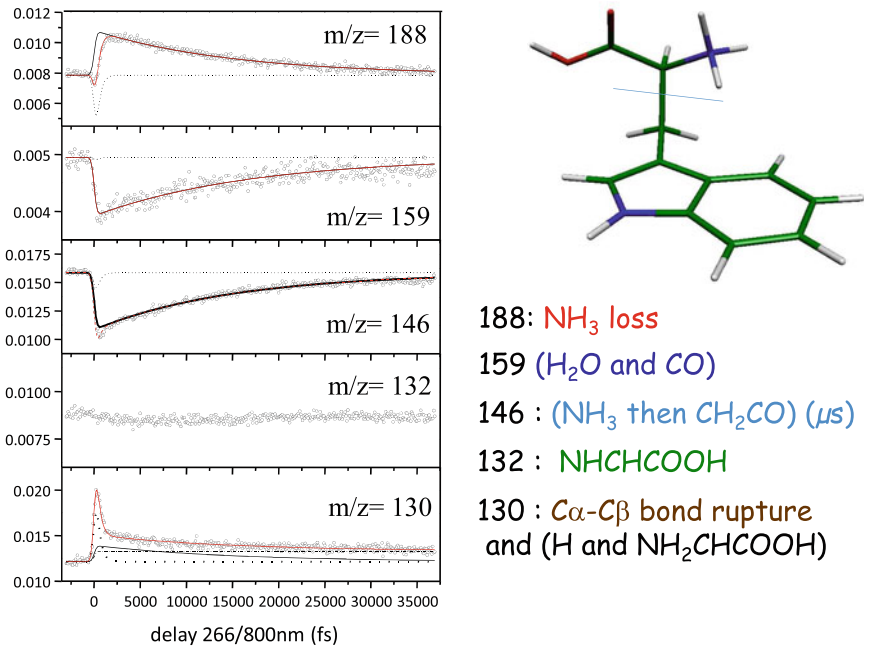

Fig. 12.1 Pump/probe experiment on protonated tryptophan (m/z 205) [8]. This is an example of how time-resolved femtosecond pump/probe experiments on protonated molecules can be complicated: each fragment has its own temporal signature, but at this timescale this is due to the excited state dynamics. In particular, m/z = 132 ions (methyl indole) do not exhibit any dynamics although they are obtained by UV excitation, as for the other fragments

12.3 General Behavior of Protonated Aromatics

12.3.1 Proton (H^+) in the Aromatic Ring

The presence of a proton in an aromatic ring has two simple effects. If it is on a carbon atom, as in benzene, it changes the hybridization character from sp2 to sp3. Upon electronic excitation, this will induce out-of-plane bending (vide infra). The presence of a positive charge on the aromatic ring also attracts the excited electron, giving rise to charge transfer (CT) excited states.

12.3.2 Proton (H^+) on the Substituent (Amino Group)

For substituted protonated aromatic molecules, and in particular for protonated aromatic amines (from the simplest, protonated aniline, to protonated amino acid), the model [11, 12] depicted in Fig. 12.2 is the key to understanding the excited state

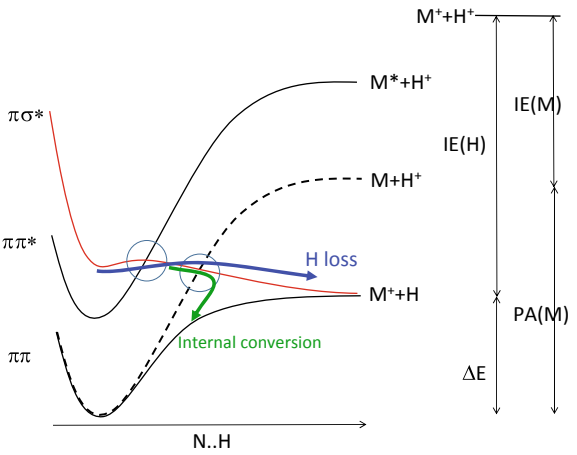

Fig. 12.2 Simple model used to understand the excited dynamics in many protonated molecules (see text)

dynamics. This ππ*/πσ* coupling model is in fact adapted from a model originally developed for neutral-substituted aromatic molecules such as phenol [13–15] or indole [16–20]. The first electronic transition corresponds to the ππ* transition that is found in all aromatic molecules. The second electronic excited state is a charge transfer state where the electron is transferred from the π orbital (located on the aromatic part, Ar) to the NH_3^+ group, leading to the formation of an hypervalent structure (Ar^+–NH_3) similar to NH_4. Recalling the original model for phenol, and due to the s character on the NH_3 group, we will call this state πσ*. As in the case of NH_4, the Ar^+–NH_3 radical is highly unstable and is dissociative along the NH coordinate. Along this coordinate, the πσ* crosses first the ππ*, and secondly, the ππ ground states. The first crossing leads to a barrier which can be passed by tunneling, and the lifetime of the ππ* state is governed by this first crossing (barrier height). The second conical intersection with the ground state leads either to an H loss or to an internal conversion, a process which is essential for the photostability of biomolecules. The variation in the lifetime of the ππ* excited state is due to the variation in the energy of the charge transfer (CT or πσ*) state relative to the optically active ππ* state. It should also be mentioned here that hypervalence on the amino group in the excited state can weaken the CN bond, potentially leading to excited state NH_3 loss (vide infra).

As illustrated in Fig. 12.2, the binding energy of a molecule in the ground state is ($E_{M+...H}$) = PA(M) + IP(M) − IP(H), where IP(H) is the H atom ionization potential (13.6 eV), PA(M) is the proton affinity of the neutral molecule, and IP(M) is its ionization potential. This binding energy also has a strong influence on the branching ratio between H loss and internal conversion pathways, and if it is larger than the energy of the ππ* state, no H loss will be observed (not enough energy to dissociate). As we will see below, this model can readily explain the behavior observed in many systems.

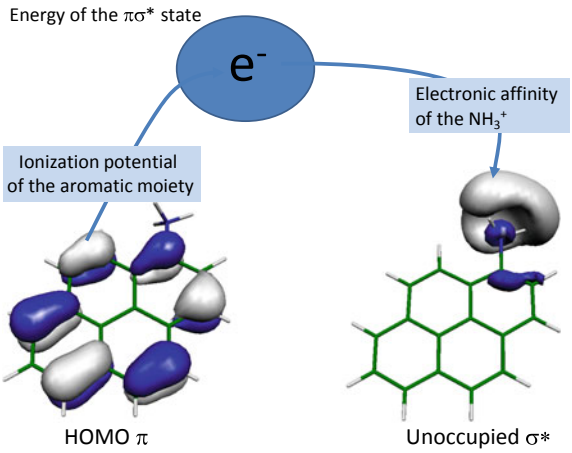

Fig. 12.3 Model to locate the πσ* state presented in the case of protonated aminopyrene

A simpler model, illustrated in Fig. 12.3, can also be used to provide further clues about the relative positions of these key states, as has been recently demonstrated [21]. We can consider that, in protonated aromatic amines, the πσ* transition corresponds to extracting an electron from the π orbital on the aromatic moiety (i.e. ionization potential of the aromatic part) and attaching it to the ammonium substituent. If we assume that the electron attachment energy on the NH_3^+ substituent ($EA(NH_3^+)$) is constant, then the πσ* energy can be deduced from the ionization potential (IP) of the neutral aromatic moiety (i.e. the aromatic without the NH_3^+ substituent, Ar) as $E_{\pi\sigma^*} = IP(Ar) - EA(NH_3^+)$. Thus, for a constant $\pi\pi^*$ energy, we can infer that a low IP of the neutral part implies a low πσ*, and thus there is a lower barrier, that is a shorter excited state lifetime.

12.4 From the Simplest to More Complex Systems

In the following section, we will review part of the work done on protonated aromatic systems, starting from the simplest (benzene) up to aromatic amino acids. Simple mechanisms that can be clearly demonstrated in simple ions will be shown to help us disentangle the processes in more complex ions.

12.4.1 Simple Aromatic Benzene/Pyridine/Pyrimidine

12.4.1.1 Benzene, Toluene

It has been shown by IR measurements that the proton [22] attached to a carbon atom of the aromatic ring creates a sp3 carbon atom in protonated benzene and toluene.

Then, upon excitation, the aromatic ring changes from a planar structure to an out-of-plane chair or boat-type structure, which leads to conical intersections with the ground state and very fast relaxation detected as structure-less excitation spectra [23, 24]. An example of the type of spectrum obtained when the proton is attached to a carbon atom of the benzene ring is shown later for 3-aminophenol (vide infra).

12.4.1.2 Pyridine, Pyrimidines

For nitrogen-containing rings, the situation is inversed. The proton linked to the nitrogen atom of the ring stabilizes the n orbital which becomes a σ orbital (see Fig. 12.4). The nπ* state becomes a σπ* state, which is no longer in the vicinity of the optically active ππ* state [25, 26]. In aromatic molecules containing two nitrogen atoms, the proton stabilizes one of the two lone pairs, and there is still a nπ* state close to the ππ* state; therefore, the out-of-plane deformation is still present and the excited lifetime is in the femtosecond regime [27]. As an example, the spectra of pyridine and pyrimidine are presented in Fig. 12.5.

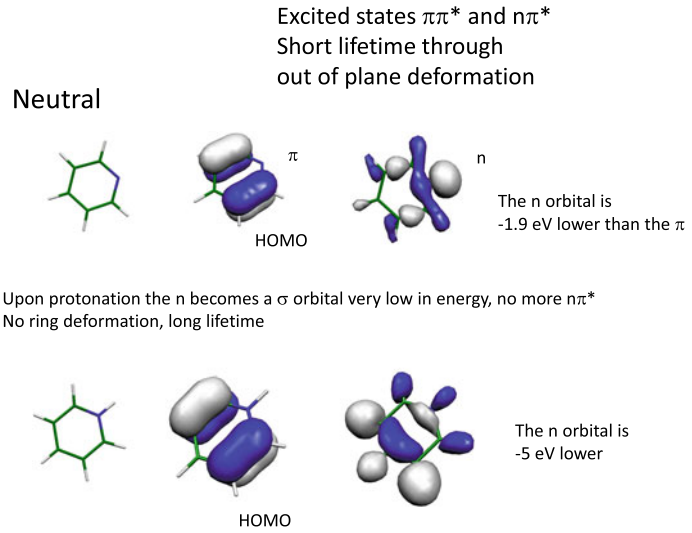

Fig. 12.4 Comparison of the orbitals in pyridine and protonated pyridine. The non-bonding n orbital in the neutral molecule becomes a much more stable σ orbital in the protonated molecule, and the σπ* state becomes higher than the ππ* state, reducing fast non-radiative processes

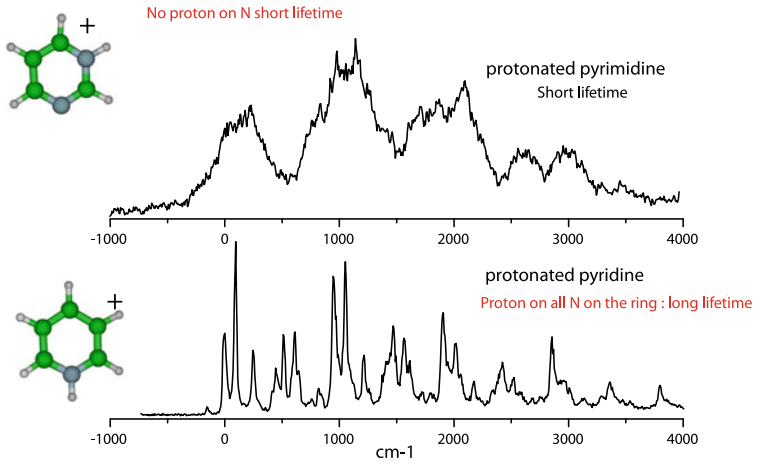

Fig. 12.5 Comparison between protonated pyridine and pyrimidine spectra. In pyridine, the lone pair on the N makes a σ bond with the proton, while in pyrimidine the lone pair on the second N is still free. The spectrum is much more congested, which is a sign of lifetime broadening and very fast (fs) excited state dynamics

12.4.2 Protonated Polycyclic Aromatic Hydrocarbons (Protonated PAH)

The electronic properties of protonated PAHs have been extensively studied by the Swiss group in Basel [28–32] and the French groups in Orsay and Marseille [33–36]. Here, the role of the charge transfer state in shifting the electronic absorption to lower energy is critical. This can be very clearly understood upon consideration of the protonated benzene dimer (Fig. 12.6). Compared to the orbitals in the neutral molecule, both the HOMO and LUMO of the protonated monomer species are stabilized by the presence of the charge in the protonated part, and the HOMO/LUMO gap remains basically the same. In the dimer, the HOMO is located on the neutral part whereas

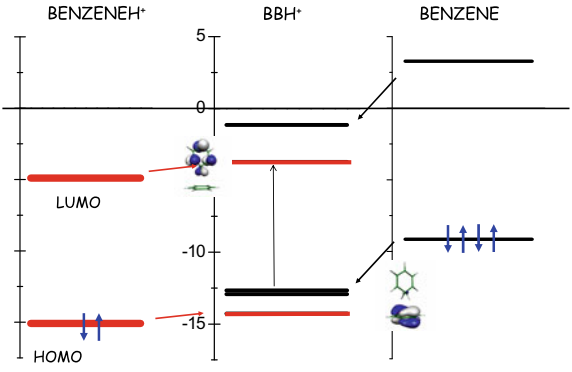

Fig. 12.6 Orbitals involved in the protonated benzene dimer. Right: HOMO and LUMO in benzene; Left: HOMO and LUMO in protonated benzene; Middle: orbitals of the protonated dimer (BBH^+)

the LUMO is on the protonated part. The first electronic transition is thus a charge transfer state from the neutral part to the protonated part, which is red-shifted compared to the transitions of both entities. As a matter of fact, the absorption of the protonated benzene (Fig. 12.7) dimer is in the visible region (450 nm, 2.75 eV) [33], compared to 4.72 eV for the neutral dimer and 3.80 eV for protonated benzene [23].

Similarly for PAH [29, 34, 37], such as naphthalene [35], anthracene [34], or even indole [38], the electron is located on the neutral part of the molecule in the ground states and on the protonated part in the first excited states. This lowers the S_1–S_0 transition by c.a. 1 eV compared to the transition in the neutral molecules.

Protonated PAHs with a nitrogen atom (PANHs) absorb in the visible or near UV spectral region. This is the same absorption region as that previously recorded for protonated PAHs with two to six aromatic rings, that is protonated naphthalene [35], anthracene [34], phenanthrene [29, 34], fluorene [37], tetracene [34], pyrene [28], and coronene [32]. The protonation of aromatic heterocycles shifts the absorption spectra to lower energy compared to the neutral molecules, but to a smaller extent than observed for the fully carbonated analogs. This corresponds to a blue shift of the transition of protonated acridine and phenanthridine compared to protonated anthracene and phenanthrene. However, protonation still leads to red shifts from the neutral homologues: for example, the S_1–S_0 transition in acridineH^+ is red-shifted by 0.4 eV from the transition in acridine, while the S_1–S_0 in anthraceneH^+ is red-shifted by 0.9 eV from the S_1–S_0 transition in neutral anthracene [39].

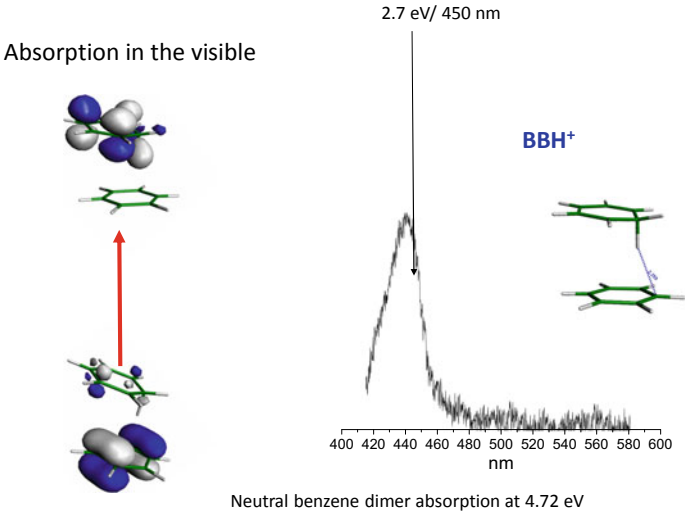

Fig. 12.7 Photofragmentation spectrum of protonated benzene dimer

12.4.3 Aromatic Amines, Aniline, Aminophenol

Many simple aromatic amines have been studied, and their behavior is well explained by the $\pi\pi^*/\pi\sigma^*$ coupling model [12, 40]. We illustrate this using the photofragmentation of protonated aminophenol as an example. For the 1-4 (*para*) isomer, two electronic states are observed (Fig. 12.8, blue line): one well-structured spectrum appears in the 4.5 eV region, very similar to the $S_1 \leftarrow S_0$ transition of the neutral molecule, while at higher energy (>5 eV) the observed structure-less continuum is assigned to the direct excitation of the $\pi\sigma^*$ state. For the 1-2 (*ortho*) isomer (Fig. 12.8, black line), the $\pi\pi^*$ state exhibits a rich low-frequency vibrational structure due to the steric hindrance between the hydroxyl and ammonium (NH_3^+) groups. This geometrical constraint also has the effect of pushing the $\pi\sigma^*$ state to higher energy and it is no longer observed. The spectrum of the 1-3 (*meta*) isomer is drastically different from the other two isomers (Fig. 12.8, red line), being strongly red-shifted and exhibiting broadened vibrational structures. This spectrum presents strong similarities to the spectra of protonated benzene or toluene, and is clearly the sign of protonation on a carbon atom of the aromatic ring. The width of the vibrational bands can be assigned to lifetime broadening, which indicates a fast electronic relaxation as predicted by ab initio calculations for protonated benzene [24]. It should also be mentioned that calculations are not very reliable for this system. At the mp2 level, the

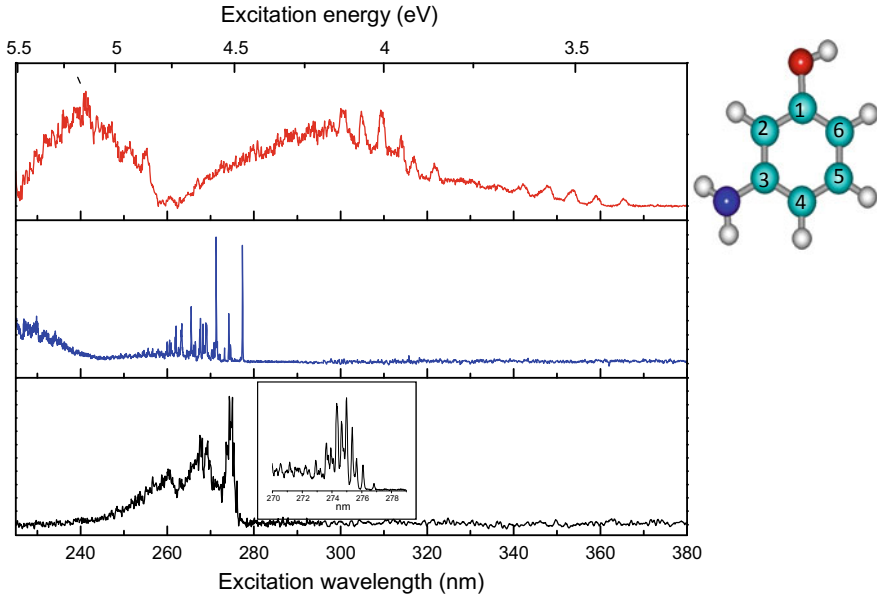

Fig. 12.8 Photofragmentation spectra of the three isomers of protonated aminophenol, with the numbering system for the atoms illustrated at the top right. Upper trace (red), the 1-3 isomer; middle trace (blue), spectrum of the 1-4 isomer; lower trace (black), spectrum of the 1-2 isomer. The insert is a zoom of the region around the 0-0 band, showing the low-frequency vibrations

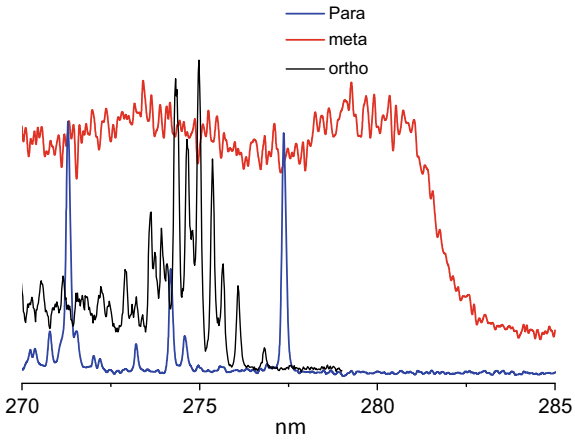

Fig. 12.9 Comparison of the photofragmentation spectra obtained for protonation on the amino group of aminophenol. In blue the 1-4, in black the 1-2, and in red the 1-3 protonated aminophenol

energy of the protonation site on the amino group and the C6 carbon atom are similar, whereas protonation on the C6 site is more stable by 0.5 eV at the DTF/B3LYP level. An added complexity is that the experimental results cannot be used to help in reconciling the two calculations, since the NH_3^+ tautomer is observed to become the most abundant one when the electrospray source conditions are changed. It is thus worthwhile to mention that the electrospray source does not necessarily produce the most stable tautomers, and that the production of one or other tautomer is very sensitive to uncontrolled parameters such as the position of the needle in front of the capillary of the source [41–43]. Thus, experimental results cannot necessarily resolve discrepancies between calculation methods.

In this example, upon changing the ESI conditions (by increasing the pressure in the capillary), 1-3 aminophenol becomes mainly protonated on the amino group. Its spectrum is compared with the spectra of other isomers in Fig. 12.9. Instead of a well-structured spectrum, as for the 1-2 and 1-4 isomers, no vibrational structure appears. Ab initio calculations, in particular the excited state optimization, show that the $\pi\pi^*$ excited state relaxes without barrier to the NH_3 loss channel after out-of-plane deformation, which allows coupling between the $\pi\pi^*$ and the $\pi\sigma^*$ states. This direct dissociation is one of the channels expected when the C–NH_3 group becomes hypervalent upon the addition of the electron (the other channel being H loss), but this is the only case where it has been observed so clearly.

12.4.4 Phenylethylamine, Tyramine [44]

Before moving to the more complex aromatic amino acids, we will first present the results for protonated phenylethylamine and tyramine.

In the most stable structure of protonated phenylethylamine (PEA, see Fig. 12.10, Φ–$CH_2CH_2NH_3$) [12] the alkyl chain is long enough that the amino group lies

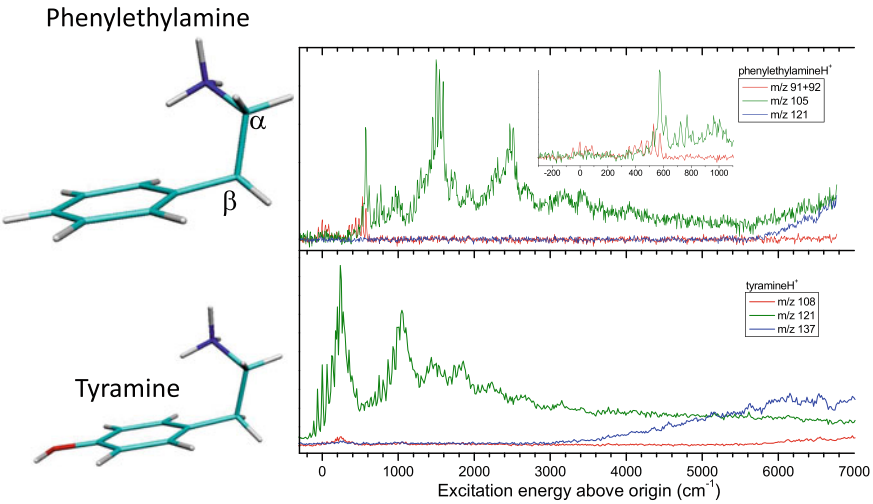

Fig. 12.10 Photofragmentation spectra of protonated phenylethylamine (upper traces) and tyramine (lower traces). In addition to the H (blue) and NH_3 loss (green) channels observed for smaller protonated aromatic amines, a new fragment appears, corresponding to C_α–C_β bond cleavage (red)

above the aromatic ring, pointing toward the C2 atom. In this system, in addition to the fragmentation channels (NH_3 and H loss) observed for shorter alkyl chains (aniline, aminophenol, benzylamine), the cleavage of the C_α–C_β bond is observed, leading to CH_2NH_3 loss (see Fig. 12.10, upper panel). The interaction of the NH_3^+ with the aromatic ring is very sensitive to the charge distribution in the ring, which changes between the ground and the $\pi\pi^*$ excited states. This is the reason for the low-frequency vibrations observed in the spectra, which correspond to NH_3^+ pseudo rotation and to rotations along the C_α–C_β bond. From ab initio calculations, the C_α–C_β bond dissociation is triggered by a proton transfer from the ammonium group toward the C2, followed by the C_α–$C_\beta H_2NH_3$ bond dissociation [44]. This channel disappears in the PEA when excess energy in S_1 is larger than 600 cm^{-1}, indicating that this channel is no longer competitive with the other channel (NH_3 loss via interconversion to the ground state). Both channels are controlled by barriers of different heights, which also determine the excited state lifetimes. For tyramine, these lifetimes have been measured, and decrease from 2/3 ns for the 0-0 band to 300 ps at 800 cm^{-1} [44].

12.4.5 Tautomers and Electronic Spectroscopy of Protonated Amino PAHs

For larger amino PAHs, both protonation on the amino group and on a carbon atom of the polycyclic aromatic moiety have been observed [21, 45]. As one would expect

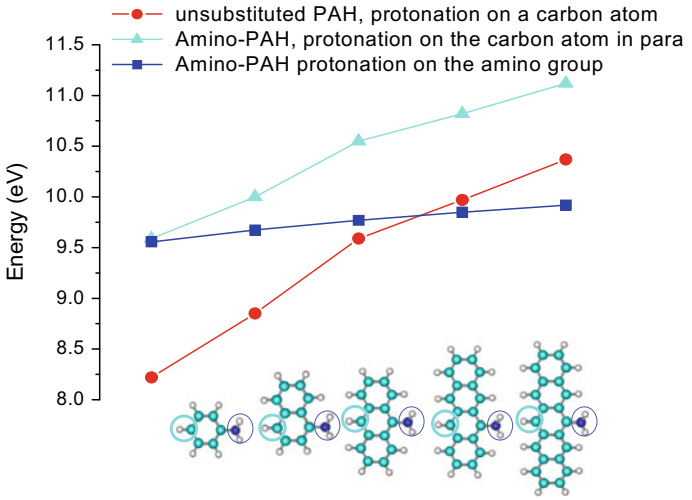

Fig. 12.11 Evolution of the proton affinity (PA) versus the PAH size. In red, the PA of the unsubstituted PAH; in dark blue, the PA for protonation on the amino group; and in light blue, the PA for protonation of the carbon atom in the para position. For aminopentacene, the proton affinity can reach 11.1 eV

from the studies mentioned above, protonation on the amino group leads to an absorption in a spectral region similar to that of the neutral molecule, whereas protonation on a carbon atom of the PAH moiety gives rise to quite strongly red-shifted transitions. The ab initio excited state calculations using either CC2 or TD/DFT are accurate enough to assign the electronic spectra to different tautomers with reasonable confidence. For large amino PAHs, calculations show that the proton affinity on aromatic carbon atoms increases strongly with the size of the PAH (see Fig. 12.11). A carbon atom on the aromatic rings rapidly becomes the most stable protonation site, and these species become very strong bases, that is "proton sponges".

12.4.6 Protonated Aromatic Amino Acids, Phenylalanine ($PheH^+$), Tyrosine ($TyrH^+$), Tryptophan ($TrpH^+$)

The excited states of protonated aromatic amino acids are probably the most studied protonated aromatic systems. As for other small aromatic amines, protonation occurs on the amino group. The first study was the femtosecond measurement of the excited lifetimes of protonated tryptophan, tyramine, and tyrosine upon excitation at 266 nm. It was found that the lifetime was in the femtosecond regime for protonated tryptamine [7] and $TrpH^+$, and in the picosecond regime for $TyrH^+$ [8, 46, 47]. It was also observed that H loss was a major fragmentation channel and, since protonation occurs on the amino group as for other small aromatic amines, the $\pi\pi^*/\pi\sigma^*$

coupling model described above was postulated, followed by later confirmation by ab initio calculations [48–50]. The pioneering experiment employing a cold ion trap [51, 52] demonstrated that the electronic spectrum could be resolved for protonated Tyr but not for $TrpH^+$, again indicating a very short excited lifetime in the latter. A well-defined photofragment spectrum for $TrpH^+$ was obtained when two water molecules were attached to the amino group [53], which is a clear indication that the lifetime becomes longer when the H loss channel is blocked and that the dynamics is controlled by the H atoms of the amino group.

12.4.6.1 Protonated Phenylalanine and Tyrosine

In this section, we will concentrate mainly on protonated tyrosine, which has been extensively studied [8, 46, 54], and on the low energy region—near the 0-0 transition—which has been characterized by many groups [52, 55–58].

Figure 12.12 presents the photofragmentation spectra for protonated tyrosine and phenylalanine over a large spectral domain. The main observed dissociation fragments are H loss, C_α–C_β bond cleavage, and $CO + H_2O$ loss. Some smaller fragments can also be seen, and these have been assigned to secondary fragmentations. Interest-

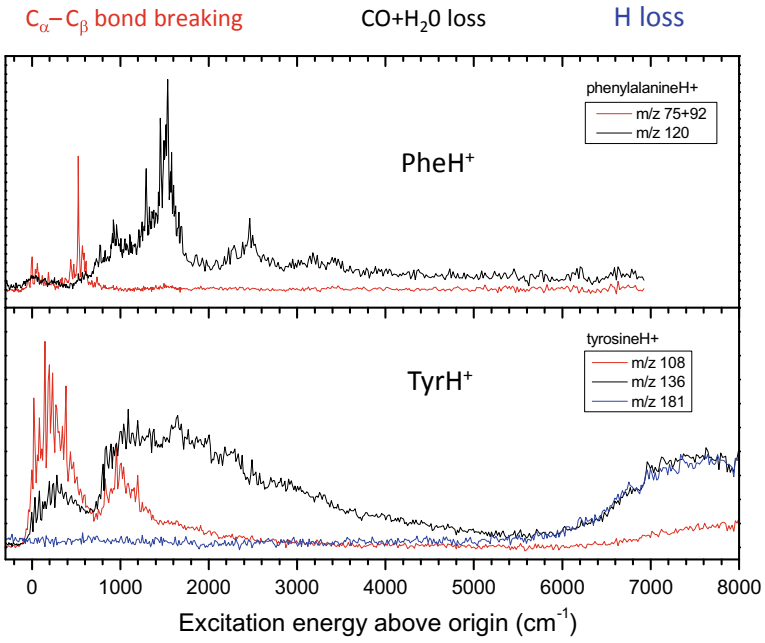

Fig. 12.12 Photofragmentation spectra of protonated phenylalanine and tyrosine over a large spectral range : Cα–Cβ bond cleavage in red, $CO + H_2O$ loss in black, H loss in blue

ingly, the presence of the carbonyl group induces a specific fragmentation channel, that is, CO + H_2O loss.

At low energy, the cleavage of the C_α–C_β bond is the predominant channel, while at higher energy the loss of CO + H_2O becomes the dominant channel and lastly, for $TyrH^+$ (but not in the case of $PheH^+$), the H loss channel appears at high energies. This can be readily explained using the $\pi\pi^*/\pi\sigma^*$ coupling model described in Sect. 12.3.2: the H loss is the result of the direct excitation of the $\pi\sigma^*$ state. The energy of this state is directly related to the ionization potential of the aromatic moiety. The IP of the phenyl or benzene is 9.24 eV, whereas the IP of phenol is 8.5 eV and thus the $\pi\sigma^*$ is 0.74 eV lower in $TyrH^+$ than in $PheH^+$. It is interesting to note that the simple model developed for larger amino-substituted PAH [21]—in which the energy of the $\pi\sigma^*$ state can be obtained from the IP of the aromatic ring minus the electronic affinity of the NH_3^+ group (3.2 eV)—predicts an energy of 8.5 − 3.2 = 5.3 eV for the $\pi\sigma^*$ state in $TyrH^+$, which is in excellent agreement with the observed onset of the H loss channel at 5.25 eV. For $PheH^+$, the same calculation predicts an energy of 6 eV for the $\pi\sigma^*$, that is out of the scanning range of the lasers (<5.5 eV). The low IP of indole (7.8 eV) in fact implies that the $\pi\sigma^*$ in $TrpH^+$ should be even lower, so that reaction barriers are very small or inexistent, and are in agreement with the femtosecond lifetime observed for the excited state. These estimated values are in good agreement with more sophisticated calculations [57], as can be seen in the calculated excited states presented in Fig. 12.13, where it is clear that the $\pi\pi^*/\pi\sigma^*$ gap is much smaller in $TrpH^+$ than in $TyrH^+$.

Four $TyrH^+$ conformers (two for $PheH^+$) have been identified through IR-UV hole-burning spectroscopy [55, 58] and they correspond to rotations of the C_α–C_β bond, with the NH_3^+ group pointing either to the C2 (stack conformer) or to the C5 (rot conformer) carbon atoms of the ring, and each with the syn- and anti-orientations of the hydroxyl group (see Fig. 12.14). A surprising result [52, 55] is that the fragmentation branching ratio is conformer-dependent, the C_α–C_β fragmentation being more important in the rot than in the stack conformer. Excited state lifetime and ab initio calculations [57] have allowed the rationalization of these results, with the model developed in the beginning of this chapter being the key to the interpretation. Compared to the protonated aromatic amines discussed earlier, the system is of higher complexity due to the presence of another charge transfer state for which the electron is located on the carbonyl group. The three H atoms of the ammonium group have differing interactions with their neighboring groups: one atom is in interaction with a carbon atom of the aromatic ring; one is hydrogen bonded to C=O; and one is free. There is also a correlation between the H atom dynamics and the electron localization. Upon electronic excitation, the H atom is going to be transferred either to the ring (if the electron stays in the $\pi\pi^*$ state, and this leads to the C_α–C_β bond cleavage), or to the C=O (if the electron is in the CT state located on the CO, and this leads to the CO + H_2O loss), and finally if the electron goes into the $\pi\sigma^*$ state on the free H atom, then that leads to the H loss channel. The rates of these processes are controlled by barriers which make the lifetime of the excited state quite long [59] (1 ns on the 0-0 with some conformer dependency), and the height of the barrier is also conformer-dependent. The success of the model was in explaining why the

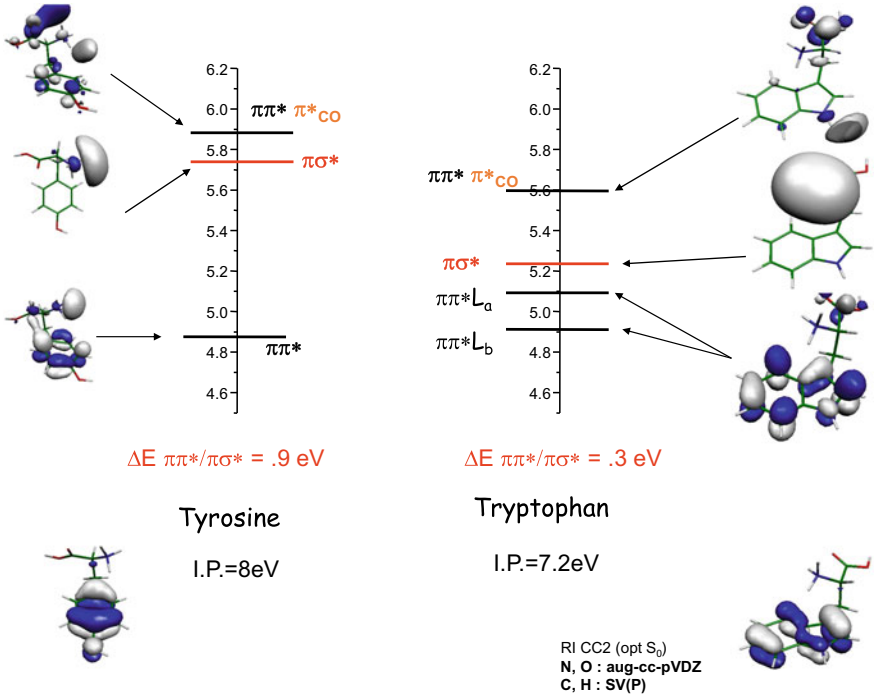

Fig. 12.13 Excited states and orbitals in protonated Tyr and Trp obtained at the CC2/aug-cc-pVDZ level [49]—The $\pi\pi^*$ state is the lowest excited state. At higher energy, two charge transfer states are present, corresponding to electron transfer to the NH_3 group or to the C=O group

C_α–C_β fragmentation channel is more important for the stack conformer than for the rot: this effect is not related to the change in the barrier for H transfer to the ring, but rather to the barrier for H transfer to CO which is higher in the rot conformer, in turn favoring H transfer to the ring and C_α–C_β cleavage (Fig. 12.14). This interpretation relies on ab initio calculations performed at the CC2/aug-cc-pVDZ level, and the validity of the method has been tested by comparing the calculated electronic spectra (vibration and Franck–Condon factors) with the experiment for each conformer, in which case the agreement is quite good [57, 58].

For protonated phenylalanine, the same stack and rot conformers have been observed, but no variation in the fragmentation channels with the conformer is seen, which is in agreement with the absence of variation in the barrier heights upon the C_α–C_β rotation.

12.4.6.2 Protonated Tryptophan

Low-resolution photofragmentation spectra of $TrpH^+$ were first recorded at room temperature [50] or in a trap cooled to the temperature of liquid nitrogen [46]. The

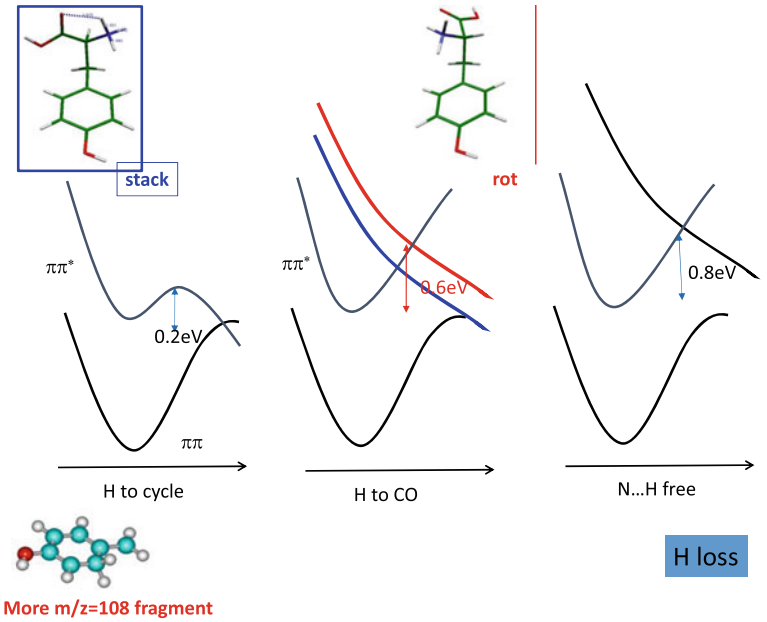

Fig. 12.14 Potential energy curve for the excited states of protonated tyrosine along the three coordinates NH to cycle, NH to CO, and NH free. Left: H transfer to the cycle through a barrier of 0.2 eV in the ππ* state. Middle: H transfer toward the C=O. The ππ*is a bond state along this coordinate. It crosses the CT_{CO} state, leading to a crossing at 0.6 eV above the origin of the ππ*state in the rot conformer (red curve) and at 0.4 eV in the stack conformer (blue curve). This explains the change in fragmentation branching ratio between the two conformers. Right: H transfer to the πσ* on NH, leading to H loss

absorption region is similar to that of the indole chromophore. At lower temperature, the spectrum is still broad [51, 53], reflecting the short excited state lifetime, but it is spectrally well resolved when the H motion of the NH_3^+ group is blocked by water molecules. The fragmentation pattern is more complex than for $TyrH^+$, as shown in Figs. 12.1 and 12.15.

The time dependences of the fragmentation of protonated amino acids and peptides upon UV excitation have been measured in an electrostatic ion storage ring. These measurements allow the detection of fragmentation occurring for a very long time [60]. After absorption of a 266 nm photon, protonated Trp has a lifetime of 10–20 ms. Using fast ion beams and ion neutral coincidences, the fragmentation dynamics have been extensively studied [61–63]. It was shown that the dynamics at very long times are due to the fragmentation of the radical obtained after the H loss (leading to the m/z = 130 fragment, methyl indole ion radical minus H). The ion neutral coincidence technique has also provided the possibility to measure whether a fragmentation occurs in one step or is a two-step process. It was shown that CO + H_2O loss is a two-step process, with CO loss occurring first, followed by H_2O

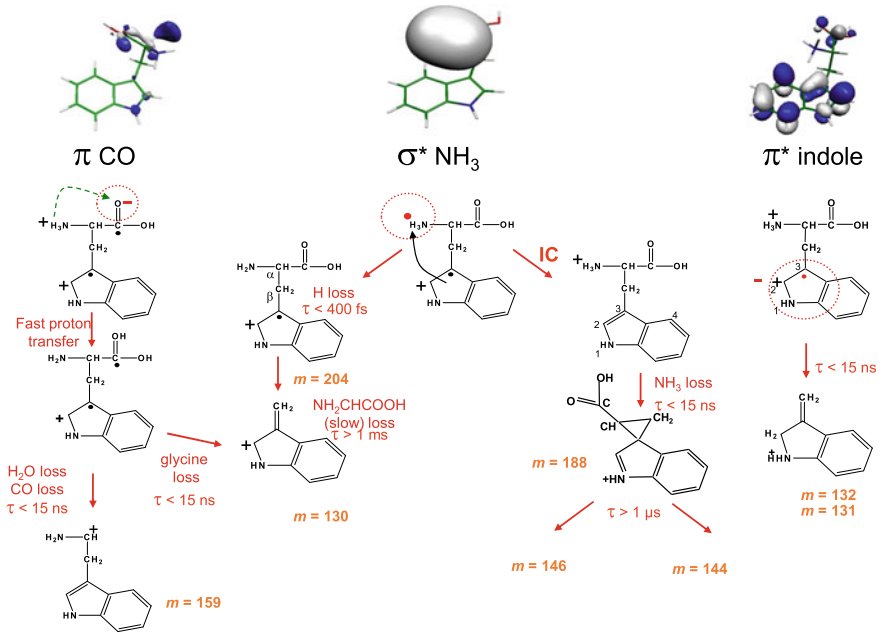

Fig. 12.15 Simplified fragmentation pathways for the fragmentation dynamics of protonated tryptophan. Adapted from Lepere et al. [62], with the permission from AIP Publishing

loss, as well as that the fragment m/z 132 (protonated methyl indole) is obtained in a one-step process. The overall picture is given in Fig. 12.15.

From the femtosecond experiment [8] and the ab initio calculations [48, 49], and similarly to tyrosine, a picture of a photofragmentation dynamics dependent on which excited state the electron is transferred to has emerged [10]:

- The $\pi\pi^*$CO state leads to two deactivation pathways. A barrierless H transfer from the NH_3^+ group to the carbonyl group within 400 fs. The concerted electron-proton transfer to the carbonyl weakens the C_α–C_β bond and could lead to the fragmentation channel at mass m/z = 130 (glycine loss). In the second path, the excess electron on the carbonyl can lead to the CO+H_2O loss channel.
- The $\pi\sigma^*$ state leads to H loss through a barrier within 15 ps. This in turn leads to the formation of the radical cation at mass m/z = 204 that can further fragment into its secondary fragment ion at mass m/z = 130 (slow fragmentation). In the absence of H loss, due to a second crossing with the ground state leading to an internal conversion, NH_3 loss will occur, followed by further fragmentation.
- The $\pi\pi^*$ state leads to a proton transfer from the NH_3^+ group to the indole ring. The fragment ion associated with this proton transfer reaction is m/z = 132. This channel is not in competition with the other ones, as evidenced by the absence of femtosecond dynamics (see Fig. 12.1). Indeed, it has been shown [7] that femtosecond dynamics are only observed if there is a competition between fragmentation

channels. In other words, some conformers (the experiment is done at room temperature) fragment only through this channel.

12.4.6.3 The Role of Triplet States

In larger peptides, dissociation through the triplet state seems to be observed upon UV excitation followed by IR multiphoton dissociation at long delay [64] for the C_α–C_β bond cleavage channel: fragmentation increases strongly when the IR laser is sent after the UV laser. In aromatic amino acids, this effect should have been seen in pump/probe experiments, as for substituted pyridine (vide infra) it is not yet the case. The open question is thus: what makes the difference between amino acids and larger peptides? Another question remains: what is the lifetime of the "collision complex" obtained after the bond cleavage? When the chemical bond breaks, the neutral and ion fragments are still bonded by the ion/molecule interaction, which is not negligible. It requires then some tens of nanoseconds [65] for room temperature ions to fragment and it might be much longer at very low temperature. It may then be possible to characterize the collision complex, which might be partly responsible for this IR effect.

12.4.7 DNA Bases and Substituted Pyridine

Very fast relaxation of the excited states to the ground state in DNA/RNA bases is a necessary process to ensure the photostability of DNA, and its rate is highly sensitive to the tautomeric form of the bases. Protonation of the bases plays a crucial role in many biochemical and mutagenic processes and can result in alternative tautomeric structures, and thus having knowledge of the properties of protonated DNA/RNA bases is very important.

The fragments observed upon photofragmentation are the same as in collision-induced dissociation, and therefore, it is highly likely that there is internal conversion to S_0 followed by fragmentation. The photofragmentation spectra of protonated DNA/RNA bases [66–69] obtained at low temperature in ion traps are all displayed together in Fig. 12.16. For cytosine and uracil, two band systems are clearly observed, and these have been shown to belong to different tautomers through UV/UV hole-burning experiments. Since these band systems are well separated, the assignment of the different tautomers can be obtained from the excited state calculations. Accurate comparison between experiment and calculations usually necessitates the calculation of the adiabatic S_1–S_0 transition as well as vibrational modes in the ground and excited states. However, excited state optimization is very difficult for these ions due to the presence of multiple out-of-plane deformations which lead to many potential energy curve crossings.

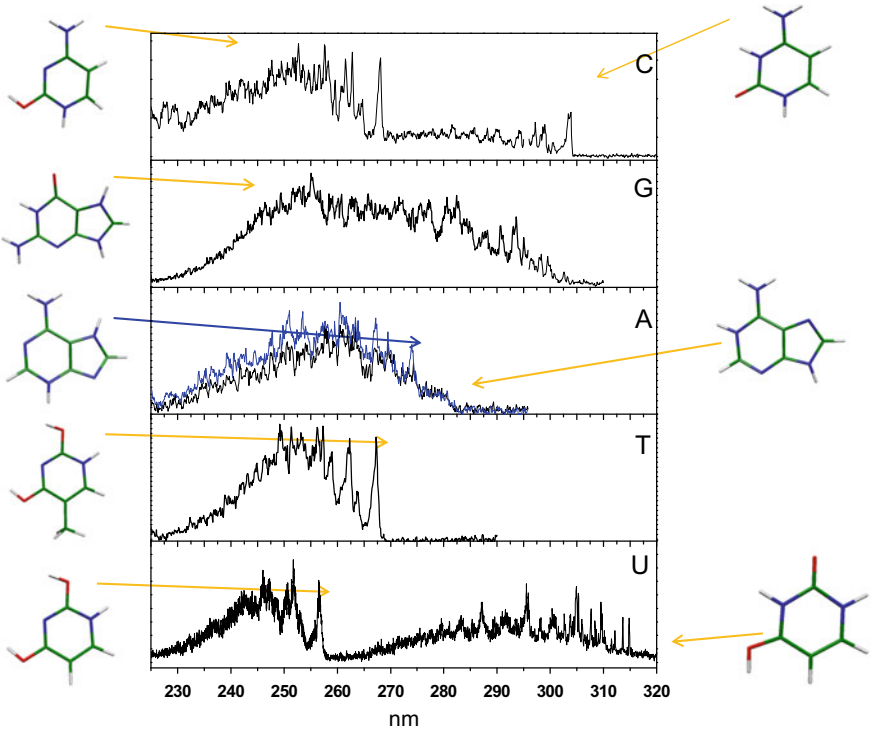

Fig. 12.16 Photofragmentation spectra for protonated DNA bases. From top to bottom: CytosineH$^+$, GuanineH$^+$, AdenineH$^+$, ThymineH$^+$, UracilH$^+$

Instead, an empirical "rule" based on many calculations can be used: as a general trend, the excited state optimization process for aromatic molecules (neutral or protonated) leads to a stabilization of c.a. 0.5 eV compared to the vertical excitation energy (E_{vert}), with 0.3 eV coming from the S_1 optimization and 0.2 eV from the change in the vibrational zero-point energy between the ground and excited state vibrational modes. As an example, for the enol/1H–2H tautomer of cytosineH$^+$, E_{vert} is 5.15 eV (calculated at the CC2/cc-pVDZ level) and the stabilization is expected to lead to an adiabatic transition energy $E_{ad} = E_{vert} - 0.5$ eV $= 4.65$ eV, which is in very good agreement with the experimental value (4.63 eV) and the calculated adiabatic transition energy (4.62 eV).

12.4.7.1 Adenine

The photofragmentation spectra of protonated DNA bases were first obtained for adenine recorded at the temperature of liquid nitrogen. The measured spectrum was very broad and structure-less [68]. This absence of structure was mainly due to fast

non-radiative decay in the system, as shown by pump/probe experiments, where the lifetime was determined to be smaller than the laser resolution of 160 fs [9]. This lifetime is a lot shorter than the lifetime of neutral adenine [69]. The photofragmentation spectrum obtained at lower temperature [66] (30 K) exhibits some vibrational structure with very broad bandwidths (180 cm^{-1}). A similar spectrum recorded for guanine exhibits a vibrational bandwidth of 12 cm^{-1} (see Fig. 12.17). The broadening in adenine was then assigned to lifetime broadening, leading to the determination of an excited state lifetime of 30 fs. For protonated adenine, another broader structure underlies the vibronic bands, and this should belong to another tautomer with an even shorter lifetime. On the basis of ab initio calculations, the tautomers were assigned to the 1H–9H and the 3H–7H structures [66]. Ab initio calculations have shown that many deformations can lead to conical intersections to the ground state, responsible for the non-radiative processes [68]. It is interesting to note that these

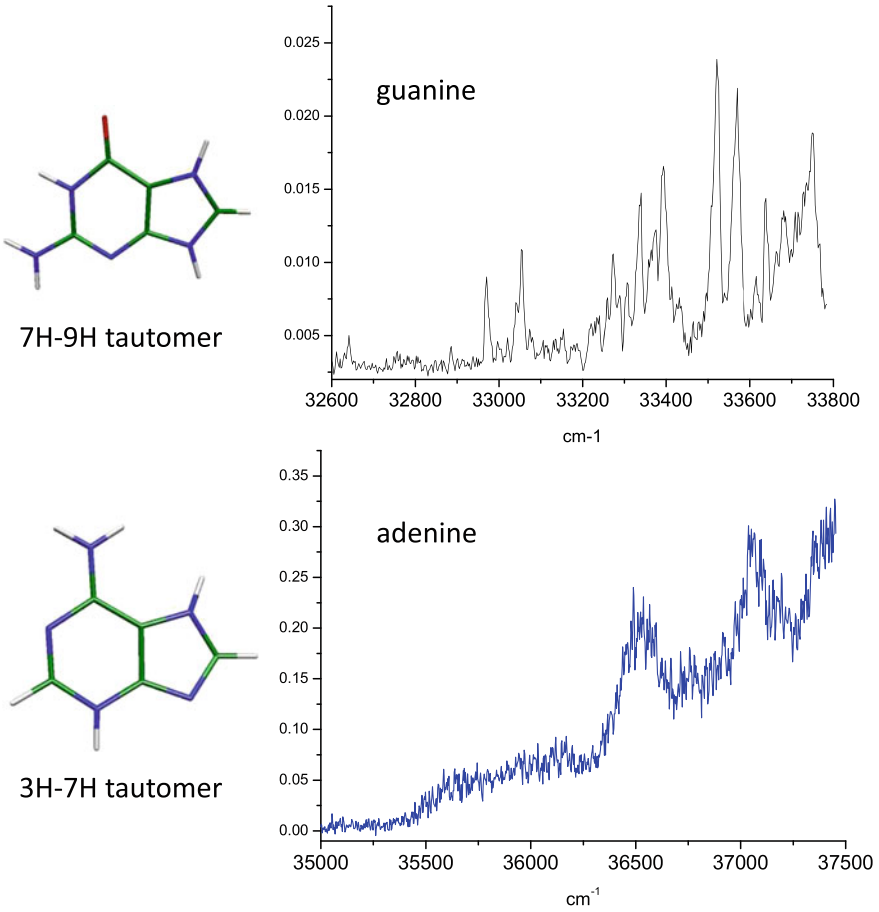

Fig. 12.17 Protonated guanine (top) and adenine (low) fragmentation spectra

very fast processes are partially suppressed in the protonated adenine dimer [70] or in adenineK^+ [71].

12.4.7.2 Guanine

In the case of protonated guanine, the ground state of the 7H–9H tautomer has been shown to be more stable by at least 23 kJ/mol (0.24 eV) compared with the other tautomers. The observed spectrum can be assigned to this tautomer by comparison with calculations, using the empirical rule ($E_{ad} = E_{vert} - 0.5$ eV). The spectrum presents well-resolved vibrational bands that can be followed for more than 1000 cm^{-1} without any sign of spectral broadening, indicating the absence of very fast relaxation processes.

12.4.7.3 Protonated Pyrimidine Bases

In the pyrimidine bases, two tautomers have been observed for uracil and cytosine, which have nearly the same energy in the ground state. In the case of thymine, only the enol/enol form is seen, probably because the difference in energy with the enol/keto is larger (0.17 eV). The excited state lifetimes deduced from the broadening of the bands are short, 100 fs or less, except for the enol/keto form of protonated uracil (low-energy band system U (red) in Fig. 12.18). In the latter case, the bandwidth is limited by the laser and the rotational envelope. As mentioned earlier for protonated pyrimidine, if the nitrogen atoms in the ring are bound to the proton/hydrogen, it pushes the $n\pi^*$ state to higher energies and decreases the non-radiative processes. One would then imagine that the keto/keto form of cytosineH^+ should have a long lifetime, but in fact the lifetime was measured to be in the order of 100 fs, showing that another non-radiative channel linked to the amino group opens.

12.4.7.4 Excited State Dynamics of Cold Protonated Cytosine Tautomers [72]

The excited states dynamics of protonated cytosine tautomers have been revisited by characterizing the dynamics from femtoseconds to milliseconds via a novel pump/probe photodissociation scheme applied to cryogenic ion spectroscopy. The very short lifetime range is extracted from spectral broadening; the nanosecond range from picosecond pump/probe experiments; and the fragmentation time in the microseconds to milliseconds time range is obtained with electronically synchronized nanosecond lasers, applying a delay between the laser pulse and the extraction of the ions from the trap. In this molecule, the locally excited $^1\pi\pi^*$ state decays on a femtosecond timescale to long-lived charge transfer and triplet states with life-

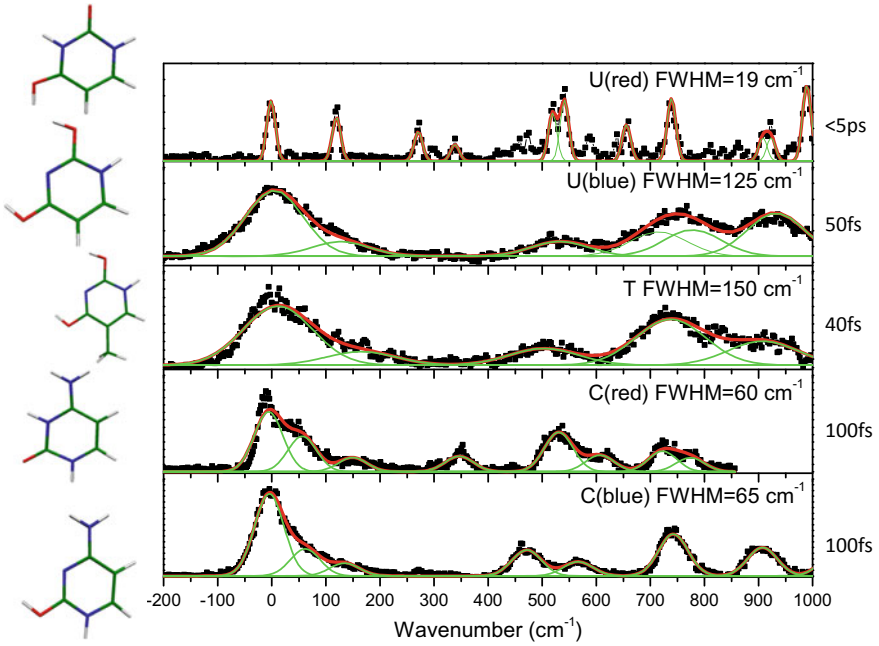

Fig. 12.18 Comparison between the different tautomers of the pyrimidine protonated DNA bases uracil (U), thymine (T) and cytosine (C). From the spectral broadening, the excited state lifetimes can be deduced. For uracil enol/keto, the width of the vibrational levels is limited by the laser bandwidth

times ranging from microseconds to milliseconds, respectively. To rationalize all the dynamics observed, a three-step mechanism (see Fig. 12.19) ($^1\pi\pi^* \rightarrow$ 1CT $\rightarrow$ $^3\pi\pi^*$) is necessary, within which internal conversion can occur from each state, ultimately leading to fragmentation in the ground electronic state. In the enol form, the $\pi\pi^*$ decays within the femtosecond range toward a charge transfer state, inducing rotation of the amino group—qualified as a twisted intramolecular charge transfer state (TICT). This TICT state then decays within the microsecond range to a triplet state, which in turn decays to the ground state, leading to fragmentation. For the keto tautomer, the fast process is a $\pi\pi^*$ transfer to a CT state in the carbonyl group (see Broquier et al. [72] for more details). A much longer lived component has also been evidenced, and was assigned to the relaxation of the CT states through intersystem crossing to the lowest $^3\pi\pi^*$ triplet state with a lifetime on the order of 10 ms for both tautomers.

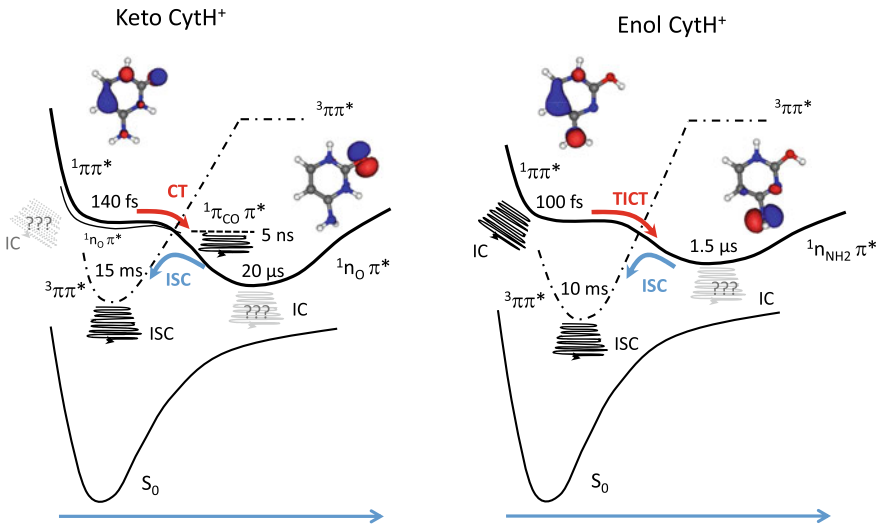

Fig. 12.19 Comparison of the decay pathways of the keto and enol tautomers of protonated cytosine. Adapted from Broquier et al. [72]. Copyright 2017 American Chemical Society

12.4.7.5 Twisted Intramolecular Charge Transfer in Protonated Aminopyridine [73]

The excited state properties of protonated *ortho*(2-), *meta* (3-), and *para* (4-) aminopyridine molecules were investigated via UV photofragmentation spectroscopy and excited state coupled-cluster CC2 calculations. Although protonated aminopyridines are rather simple aromatic molecules, their deactivation mechanisms are quite complex, yielding unexpected results. In protonated 3- and 4-aminopyridine, the fragmentation yield is negligible around the band origin, implying the absence of internal conversion to the ground state. Besides this, a twisted intramolecular charge transfer reaction was shown to be present in protonated 4-aminopyridine around the band origin, while an excited state proton transfer channel from the pyridinic nitrogen to the adjacent carbon atom opens at roughly 500 cm^{-1} of excess energy.

12.5 Conclusions

In this chapter, we have summarized the current understanding of the excited states of protonated aromatic molecules. While some general properties have been determined, allowing an appreciation of the typical behavior of these ions, the number of molecules studied to date remains limited. In particular, it has been shown that the excited state properties are strongly influenced by the presence of charge transfer states involving the extra proton, either in terms of the energy of the state—in the

case of protonation on aromatics rings—or in terms of excited state lifetimes—when the proton is on a substituent. It should be emphasized that knowledge of the optical properties of these ions creates new opportunities for the characterization of tautomers/conformers in analytical chemistry [74, 75] since, in a cold ion trap, each species has its own unique spectroscopic fingerprint. However, although there has been a recent augmentation in studies on the excited state of protonated molecules, the excited state properties of deprotonated or hydrogenated [76–78] molecules are still very little understood and this represents a major challenge for the coming years.

References

1. Freiser, B.S., Beauchamp, J.L.: Photochemistry of organic ions in the gas phase. Comparison of the gas phase photodissociation and solution absorption spectra of benzoyl cation, protonated benzene, and protonated mesitylene. J. Am. Chem. Soc. **98**(11), 3136–3139 (1976)
2. Freiser, B.S., Beauchamp, J.L.: Acid-base properties of molecules in excited electronic states utilizing ion cyclotron resonance spectroscopy. J. Am. Chem. Soc. **99**(10), 3214–3225 (1977)
3. Polfer, N.C.: Infrared multiple photon dissociation spectroscopy of trapped ions. Chem. Soc. Rev. **40**, 2211–2221 (2011)
4. Bieske, E.J., Dopfer, O.: High resolution spectroscopy of cluster ions. Chem. Rev. **100**(11), 3963–3998 (2000)
5. Polfer, N.C., Oomens, J.: Vibrational spectroscopy of bare and solvated ionic complexes of biological relevance. Mass Spectrom. Rev. **28**(3), 468–494 (2009)
6. Fuke, F., Takasu, R.: Ultra fast photochemistry ammonia clusters: formation and decay hypervalent molecular clusters containing NH_4 radical. Bull. Chem. Soc. Jpn. **68**, 3303 (1995)
7. Kang, H., Jouvet, C., Dedonder-Lardeux, C., Martrenchard, S., Charrière, C., Grégoire, G., Desfrançois, C., Schermann, J.P., Barat, M., Fayeton, J.A.: Photoinduced processes in protonated tryptamine. J. Chem. Phys. **122**(8), 1–7 (2005)
8. Kang, H., Dedonder-Lardeux, C., Jouvet, C., Grégoire, G., Desfrançois, C., Schermann, J.-P., Barat, M., Fayeton, J.A.: Control of bond-cleaving reactions of free protonated tryptophan ion by femtosecond laser pulses. J. Phys. Chem. A **109**(11), 2417–2420 (2005)
9. Nolting, D., Weinkauf, R., Hertel, I.V., Schultz, T.: Excited-state relaxation of protonated adenine. Chem. Phys. Chem. **8**(5), 751–755 (2007)
10. Grégoire, G., Lucas, B., Barat, M., Fayeton, J.A., Dedonder-Lardeux, C., Jouvet, C.: UV photoinduced dynamics in protonated aromatic amino acid. Eur. Phys. J. D **51**(1), 109–116 (2009)
11. Kang, H., Jouvet, C., Dedonder-Lardeux, C., Martrenchard, S., Grégoire, G., Desfrançois, C., Schermann, J.-P.P., Barat, M., Fayeton, J.A.: Ultrafast deactivation mechanisms of protonated aromatic amino acids following UV excitation. Phys. Chem. Chem. Phys. **7**(2), 394–398 (2005)
12. Féraud, G., Broquier, M., Dedonder-Lardeux, C., Grégoire, G., Soorkia, S., Jouvet, C.: Photofragmentation spectroscopy of cold protonated aromatic amines in the gas phase. Phys. Chem. Chem. Phys. **16**, 5250–5259 (2014)
13. Sobolewski, A.L., Domcke, W., Dedonder-Lardeux, C., Jouvet, C.: Excited-state hydrogen detachment and hydrogen transfer driven by repulsive $\pi\sigma^*$ states: a new paradigm for nonradiative decay in aromatic biomolecules. Phys. Chem. Chem. Phys. **4**(7), 1093–1100 (2002)
14. Pino, G.A., Oldani, A.N., Marceca, E., Fujii, M., Ishiuchi, S., Miyazaki, M., Broquier, M., Dedonder, C., Jouvet, C.: Excited state hydrogen transfer dynamics in substituted phenols and their complexes with ammonia: $\pi\pi^*/\pi\sigma^*$ energy gap propensity and ortho-substitution effect. J. Chem. Phys. **133**(12), 124313 (2010)

15. Dixon, R.N., Oliver, T.A.A., Ashfold, M.N.R.: Tunnelling under a conical intersection: application to the product vibrational state distributions in the UV photodissociation of phenols. J. Chem. Phys. **134**(19), 194303 (2011)
16. Dedonder-Lardeux, C., Grosswasser, D., Jouvet, C., Martrenchard, S.: Dissociative hydrogen transfer in indole $(NH_3)_n$ clusters. Chem. Com. **4**(4), 21 (2001)
17. Lippert, H., Stert, V., Hesse, L., Schulz, C.P., Radloff, W., Hertel, I.V.: Hydrogen atom transfer in indole clusters: formation dynamics of formation dynamics of (NH3)$n-1$(NH4), $n = 1$–6, fragments. Eu. Phys. J. D. **20**(3), 445–448 (2002)
18. Nix, M.G.D., Devine, aL, Cronin, B., Ashfold, M.N.R.: High resolution photofragment translational spectroscopy of the near UV photolysis of indole: dissociation via the $\pi\sigma^*$ state. Phys. Chem. Chem. Phys. **8**(22), 2610–2618 (2006)
19. Livingstone, R., Schalk, O., Boguslavskiy, A.E., Wu, G., Bergendahl, L.T., Stolow, A., Paterson, M.J., Townsend, D.: Following the excited state relaxation dynamics of indole and 5-hydroxyindole using time-resolved photoelectron spectroscopy. J. Chem. Phys. **135**(19), 194307 (2011)
20. Dian, B.C., Longarte, A., Zwier, T.S.: Hydride stretch infrared spectra in the excited electronic states of indole and its derivatives: direct evidence for the $\pi\sigma^*$ state. J. Chem. Phys. **118**(6), 2696 (2003)
21. Noble, J.A., Dedonder-Lardeux, C., Mascetti, J., Jouvet, C.: Electronic spectroscopy of protonated 1-aminopyrene in a cold ion trap. Chem. Asian J. **125**, 1523–1531 (2017)
22. Solcà, N., Dopfer, O.: Protonated benzene: IR spectrum and structure of $C_6H_7^+$. Angew. Chem. Int. Ed. **41**(19), 3628–3631. 3517 (2002)
23. Esteves-López, N., Dedonder-Lardeux, C., Jouvet, C.: Excited state of protonated benzene and toluene. J. Chem. Phys. **143**(7), 074303 (2015)
24. Rode, M.F., Sobolewski, A.L., Dedonder, C., Jouvet, C., Dopfer, O.: Computational study on the photophysics of protonated benzene. J. Phys. Chem. A **113**(20), 5865–5873 (2009)
25. Pino, G.A., Feraud, G., Broquier, M., Grégoire, G., Soorkia, S., Dedonder, C., Jouvet, C.: Non-radiative processes in protonated diazines, pyrimidine bases and an aromatic azine. Phys. Chem. Chem. Phys. **18**, 20126–20134 (2016)
26. Hansen, C.S., Blanksby, S.J., Chalyavi, N., Bieske, E.J., Reimers, J.R., Trevitt, A.J.: Ultraviolet photodissociation action spectroscopy of the N-pyridinium cation. J. Chem. Phys. **142**, 014301 (2015)
27. Delchev, V.B., Sobolewski, A.L., Domcke, W.: Comparison of the non-radiative decay mechanisms of 4-pyrimidinone and uracil: an ab initio study. Phys. Chem. Chem. Phys. **12**(19), 5007–5015 (2010)
28. Hardy, F.-X., Gause, O., Rice, C.A., Maier, J.P.: Absorptions in the visible of protonated pyrene collisionally cooled to 15 K. Astrophys. J. Lett. **778**(2), 1 (2013)
29. Garkusha, I., Fulara, J., Nagy, A., Maier, J.P.: Electronic absorption spectra of protonated anthracenes and phenanthrenes, and their neutrals in neon matrices. Astrophys. J. **728**(2), 131 (2011)
30. Garkusha, I., Fulara, J., Nagy, A., Maier, J.P.: Electronic transitions of protonated benzene and fulvene, and of C_6H_7 isomers in neon matrices. J. Am. Chem. Soc. **132**(42), 14979–14985 (2010)
31. Chakrabarty, S., Holz, M., Campbell, E.K., Banerjee, A., Gerlich, D., Maier, J.P.: A novel method to measure electronic spectra of cold molecular ions. J. Phys. Chem. Lett. **4**(23), 4051–4054 (2013)
32. Garkusha, I., Fulara, J., Sarre, P.J., Maier, J.P.: Electronic absorption spectra of protonated pyrene and coronene in neon matrixes. J. Phys. Chem. A **115**, 10972–10978 (2011)
33. Chakraborty, S., Omidyan, R., Alata, I., Nielsen, I.B., Dedonder, C., Broquier, M., Jouvet, C.: Protonated benzene dimer: an experimental and ab initio study. J. Am. Chem. Soc. **131**(31), 11091–11097 (2009)
34. Alata, I., Dedonder, C., Broquier, M., Marceca, E., Jouvet, C.: Role of the charge-transfer state in the electronic absorption of protonated hydrocarbon molecules. J. Am. Chem. Soc. **132**(14), 17483–17489 (2010)

35. Alata, I., Omidyan, R., Broquier, M., Dedonder, C., Dopfer, O., Jouvet, C.: Effect of protonation on the electronic structure of aromatic molecules: naphthaleneH^+. Phys. Chem. Chem. Phys. **12**, 14456–14458 (2010)
36. Alata, I., Broquier, M., Dedonder-Lardeux, C., Jouvet, C., Kim, M., Sohn, W.Y., Kim, S., Kang, H., Schütz, M., Patzer, A., et al.: Microhydration effects on the electronic spectra of protonated polycyclic aromatic hydrocarbons: [naphthalene-$(H_2O)_{n=1,2}$]H^+. J. Chem. Phys. **134**(7), 074307 (2011)
37. Alata, I., Broquier, M., Dedonder, C., Jouvet, C., Marceca, E.: Electronic excited states of protonated aromatic molecules: protonated fluorene. Chem. Phys. **393**, 25–31 (2012)
38. Alata, I., Bert, J., Broquier, M., Dedonder, C., Féraud, G., Grégoire, G., Soorkia, S., Marceca, E., Jouvet, C.: Electronic spectra of the protonated indole chromophore in the gas phase. J. Phys. Chem. A **117**(21), 4420–4427 (2013)
39. Noble, J.A., Dedonder, C., Jouvet, C.: The electronic spectra of protonated PANH molecules. Astron. Astrophys. **A79**, 577 (2015)
40. Féraud, G., Esteves-López, N., Dedonder-Lardeux, C., Jouvet, C.: UV spectroscopy of cold ions as a probe of the protonation site. Phys. Chem. Chem. Phys. **17**, 25755–25760 (2015)
41. Xia, H., Attygalle, A.B.: Effect of electrospray ionization source conditions on the tautomer distribution of deprotonated P-hydroxybenzoic acid in the gas phase. Anal. Chem. **88**(11), 6035–6043 (2016)
42. Flammang, R., Dechamps, N., Pascal, L., Haverbeke, Y., Gerbaux, P., Nam, P.-C., Nguyen, M.: Ring versus nitrogen protonation of anilines. Lett. Org. Chem. **1**(1), 23–30 (2004)
43. Cruz-Ortiz, A.F., Rossa, M., Berthias, F., Berdakin, M., Maitre, P., Pino, G.A.: Fingerprints of both Watson–Crick and hoogsteen isomers of isolated (cytosine-guanine)H^+ pair. J. Phys. Chem. Lett. **8**, 5501–5506 (2017)
44. Broquier, M., Soorkia, S., Grégoire, G.: A comprehensive study of cold protonated tyramine: UV photodissociation experiments and ab initio calculations. Phys. Chem. Chem. Phys. **17**(39), 25854–25862 (2015)
45. Noble, J.A., Broquier, M., Gregoire, G., Soorkia, S., Pino, G.A., Marceca, E., Dedonder-Lardeux, C., Jouvet, C.: Tautomerism and electronic spectroscopy of protonated 1- and 2-aminonaphthalene. Phys. Chem. Chem. Phys. **20**, 6134–6145 (2018)
46. Nolting, D., Marian, C., Weinkauf, R.: Protonation effect on the electronic spectrum of tryptophan in the gas phase. Phys. Chem. Chem. Phys. **6**(10), 2633–2640 (2004)
47. Kang, H., Jouvet, C., Dedonder-Lardeux, C., Martrenchard, S., Grégoire, G., Desfrançois, C., Schermann, J.-P., Barat, M., Fayeton, J.A.: Ultrafast deactivation mechanisms of protonated aromatic amino acids following UV excitation. Phys. Chem. Chem. Phys. **7**(2), 394 (2005)
48. Grégoire, G., Jouvet, C., Dedonder, C., Sobolewski, A.L.: On the role of dissociative $\pi\sigma^*$ states in the photochemistry of protonated tryptamine and tryptophan: an ab initio study. Chem. Phys. **324**(2–3), 398–404 (2006)
49. Grégoire, G., Jouvet, C., Dedonder, C., Sobolewski, A.L.: Ab initio study of the excited-state deactivation pathways of protonated tryptophan and tyrosine. J. Am. Chem. Soc. **129**(19), 6223–6231 (2007)
50. Talbot, F.O., Tabarin, T., Antoine, R., Broyer, M., Dugourd, P.: Photodissociation spectroscopy of trapped protonated tryptophan. J. Chem. Phys. **122**(7), 074310 (2005)
51. Boyarkin, O.V., Mercier, S.R., Kamariotis, A., Rizzo, T.R.: Electronic spectroscopy of cold protonated tryptophan and tyrosine. J. Am. Chem. Soc. **128**, 2816–2817 (2006)
52. Rizzo, T.R., Stearns, J.A., Boyarkin, O.V.: Spectroscopic studies of cold, gas-phase biomolecular ions. Int. Rev. Phys. Chem. **28**(3), 481 (2009)
53. Mercier, S.R., Boyarkin, O.V., Kamarioti, A., Guglielmi, M., Tavernelli, I., Cascella, M., Rothlisberger, U., Rizzo, T.R.: Microsolvation effects on the excited-state dynamics of protonated tryptophan. J. Am. Chem. Soc. **128**(51), 16938–16943 (2006)
54. Choi, C.M., Choi, D.H., Kim, N.J., Heo, J.: Effective temperature of protonated tyrosine ions in a cold quadrupole ion trap. Int. J. Mass Spectrom. **314**, 18–21 (2012)
55. Stearns, J.A., Mercier, S., Seaiby, C., Guidi, M., Boyarkin, O.V., Rizzo, T.R.: Conformation-specific spectroscopy and photodissociation of cold, protonated tyrosine and phenylalanine. J. Am. Chem. Soc. **129**(38), 11814–11820 (2007)

56. Redwine, J.G., Davis, Za, Burke, N.L., Oglesbee, Ra, McLuckey, Sa, Zwier, T.S.: A novel ion trap based tandem mass spectrometer for the spectroscopic study of cold gas phase polyatomic ions. Int. J. Mass Spectrom. **348**, 9–14 (2013)
57. Féraud, G., Broquier, M., Dedonder, C., Jouvet, C., Gregoire, G., Soorkia, S.: Excited-state dynamics of protonated phenylalanine and tyrosine: photo-induced reactions following electronic excitation. J. Phys. Chem. A **119**, 5914–5924 (2015)
58. Ishiuchi, S., Wako, H., Kato, D., Fujii, M.: High-cooling-efficiency cryogenic quadrupole ion trap and UV-UV hole burning spectroscopy of protonated tyrosine. J. Mol. Spectrosc. **332**, 45–51 (2017)
59. Soorkia, S., Broquier, M., Grégoire, G.: Conformer- and mode-specific excited state lifetimes of cold protonated tyrosine ions. J. Phys. Chem. Lett. **5**(24), 4349–4355 (2014)
60. Andersen, J.U., Cederquist, H., Forster, J.S., Huber, B.A., Hvelplund, P., Jensen, J., Liu, B., Manil, B., Maunoury, L., Nielsen, S.B., et al.: Photodissociation of protonated amino acids and peptides in an ion storage ring. Determination of Arrhenius parameters in the high-temperature limit. Phys. Chem. Chem. Phys. **6**(10), 2676–2681 (2004)
61. Lepere, V., Lucas, B., Barat, M., Fayeton, J.A., Picard, Y.J., Jouvet, C., Çarçabal, P., Nielsen, I.B., Dedonder-Lardeux, C., Grégoire, G., et al.: Characterization of neutral fragments issued from the photodissociation of protonated tryptophane. Phys. Chem. Chem. Phys. **9**(39), 5330–5334 (2007)
62. Lepere, V., Lucas, B., Barat, M., Fayeton, J.A., Picard, Y.J., Jouvet, C., Çarçabal, P., Nielsen, I.B., Dedonder-Lardeux, C., Grégoire, G., et al.: Comprehensive characterization of the photodissociation pathways of protonated tryptophan. J. Chem. Phys. **127**(13), 134313 (2007)
63. Dedonder, C., Féraud, G., Jouvet, C.: Excited-state dynamics of protonated aromatic amino acids. In: Brøndsted Nielsen, S., Wyer, J.A. (eds.) Photophysics of Ionic Biochromophores. Physical Chemistry in Action, pp. 155–180. Springer, Berlin (2013)
64. Zabuga, A.V., Kamrath, M.Z., Boyarkin, O.V., Rizzo, T.R.: Fragmentation mechanism of UV-excited peptides in the gas phase. J. Chem. Phys. **141**(15) (2014)
65. Soorkia, S., Dehon, C., Kumar, S.S., Pérot-Taillandier, M., Lucas, B., Jouvet, C., Barat, M., Fayeton, Ja: Ion-induced dipole interactions and fragmentation times: C_α–C_β chromophore bond dissociation channel. J. Phys. Chem. Lett. **6**, 2070–2074 (2015)
66. Berdakin, M., Féraud, G., Dedonder-Lardeux, C., Jouvet, C., Pino, G.A.: Excited states of protonated DNA/RNA bases. Phys. Chem. Chem. Phys. **16**, 10643–10650 (2014)
67. Pedersen, S.Ø., Byskov, C.S., Turecek, F., Nielsen, S.B.: Structures of protonated thymine and uracil and their monohydrated gas-phase ions from ultraviolet action spectroscopy and theory. J. Phys. Chem. A **118**(24), 4256–4265 (2014)
68. Marian, C., Nolting, D., Weinkauf, R.: The electronic spectrum of protonated adenine: theory and experime. Phys. Chem. Chem. Phys. **7**, 3306–3316 (2005)
69. Kim, N.J., Chang, J., Kim, H.M., Kang, H., Ahn, T.K., Heo, J., Kim, S.K.: Femtosecond decay dynamics of intact adenine and thymine base pairs in a supersonic jet. Chem. Phys. Chem. **12**(10), 1935–1939 (2011)
70. Kang, H., Féraud, G., Dedonder-lardeux, C., Jouvet, C.: New method for double-resonance spectroscopy in a cold quadrupole ion trap and its application to UV-UV hole-burning spectroscopy of protonated adenine dimer. J. Phys. Chem. Lett. **5**, 2760 (2014)
71. Baek, J.Y., Choi, C.M., Eun, H.J., Park, K.S., Choi, M.C., Heo, J., Kim, N.J.: Ultraviolet photodissociation spectroscopy of cold, isolated adenine complexes with a potassium cation. Chem. Phys. Lett. **635**, 163–167 (2015)
72. Broquier, M., Soorkia, S., Pino, G., Dedonder-Lardeux, C., Jouvet, C., Grégoire, G.: Excited state dynamics of cold protonated cytosine tautomers: characterization of charge transfer, intersystem crossing, and internal conversion processes. J. Phys. Chem. A **121**, 6429–6439 (2017)
73. Broquier, M., Soorkia, S., Dedonder-Lardeux, C., Jouvet, C., Theulé, P., Grégoire, G.: Twisted intramolecular charge transfer in protonated amino pyridine. J. Phys. Chem. A **120**(21), 3797–3809 (2016)
74. Kopysov, V., Makarov, A., Boyarkin, O.V.: Colors for molecular masses: fusion of spectroscopy and mass spectrometry for identification of biomolecules. Anal. Chem. (2015). 150406105317008

75. Kopysov, V., Makarov, A., Boyarkin, O.V.: Nonstatistical UV fragmentation of gas-phase peptides reveals conformers and their structural features. J. Phys. Chem. Lett. **7**(6), 1067–1071 (2016)
76. Krechkivska, O., Wilcox, C., O'Connor, G.D., Nauta, K., Kable, S.H., Schmidt, T.W.: Ionization energies of three resonance-stabilized radicals: cyclohexadienyl (D_n, $n = 0, 1, 6, 7$), 1-phenylpropargyl, and methylcyclohexadienyl. J. Phys. Chem. A **118**(44), 10252–10258 (2014)
77. Sebree, J.A., Kislov, V.V., Mebel, A.M., Zwier, T.S.: Spectroscopic and thermochemical consequences of site-specific H-atom addition to naphthalene. J. Chem. Phys. **114**, 6255–6262 (2010)
78. Krechkivska, O., Wilcox, C.M., Troy, T.P., Nauta, K., Chan, B., Jacob, R., Reid, S.A., Radom, L., Schmidt, T.W., Kable, S.H.: Hydrogen-atom attack on phenol and toluene is ortho-directed. Phys. Chem. Chem. Phys. **18**(12), 8625–8636 (2016)